Hexamethylenetetramine-mediated growth of grain-boundary-passivation CH3NH3PbI3 for highly reproducible and stable perovskite solar cells

Elsevier Editorial System(tm) for Journal of Power Sources

Manuscript Draft

Manuscript Number: POWER-D-17-04038R2

Title: Hexamethylenetetramine-mediated growth of grain-boundary-passivation CH3NH3PbI3 for highly reproducible and stable perovskite solar cells

Article Type: Research Paper

Keywords: Perovskite solar cell; Hexamethylenetetramine; Grain-boundary-passivation; Stability; DFT calculation

Corresponding Author: Ms. xia tao,

Corresponding Author's Institution: Beijing University of Chemical Technology

First Author: Yan-Zhen Zheng

Order of Authors: Yan-Zhen Zheng; Xi-Tao Li; Er-Fei Zhao; Xin-Ding Lv; Fan-Li Meng; Chao Peng; Xue-Sen Lai; Meilan Huang; Guozhong Cao; xia tao; Jian-Feng Chen

Abstract: Simultaneously achieving the long-term device stability and reproducibility has proven challenging in perovskite solar cells because solution-processing produced perovskite film with grain boundary is sensitive to moisture. Herein, we develop a hexamethylenetetramine (HMTA)-mediated one-step solution-processing deposition strategy that leads to the formation of high-purity and grain-boundary-passivation CH3NH3PbI3 film and thereby advances cell optoelectronic performance. Through morphological and structural characterizations and theoretical calculations, we demonstrate that HMTA fully occupies the moisture-exposed surface to build a bridge across grain boundary and coordinates with Pb ions to inhibit the formation of detrimental PbI2. Such HMTA-CH3NH3PbI3 films achieve a decent augmentation of power conversion efficiency (PCE) from 12.70% to 17.87%. A full coverage of PbI2-free CH3NH3PbI3 surface on ZnO also boosts the device's stability and reproducibility.

Re: Submission of Revised Manuscript (POWER-D-17-04038R2)

Dear editor,

We are pleased to re-submit an electronic version of our revised manuscript (MS. NO: POWER-D-17-04038R2) entitled by “Hexamethylenetetramine-mediated growth of grain-boundary-passivation $CH_3NH_3PbI_3$ for highly reproducible and stable perovskite solar cells” by Yan-Zhen Zheng, Xi-Tao Li, Erfei Zhao, Xin-Ding Lv, Fan-Li Meng, Chao Peng, Xue-Sen Lai, Meilan Huang, Guozhong Cao, Xia Tao and Jian-Feng Chen. All revised/supplemented sections are labeled in blue (see revised MS).

Please kindly contact us by e-mail or fax if you have any other problems.

With best regards.

Sincerely yours,

Prof. Dr. Xia Tao

P.O.Box 35

15 Bei San Huan East Road

Beijing University of Chemical Technology

Beijing 100029, China

Tel: +86-10-6445-3680

Fax: +86-10-6443-4784

E-mail: taoxia@yahoo.com

Response to reviewer comments

Referee 1

Comments: As authors have answered most of the queries, hence I do not have objection for its appearance in the journal. Moreover, the authors should check the citation of all figures in the main text shown in supporting information, for example page 10, Fig S4 may be Fig S6 and page 17, Fig 10 may be Fig 12.

Response: We thank for the appreciation of the Referee 1. We have carefully checked and corrected the citation of Figures in the main text displayed in supporting materials accordingly (See P. 10 & 17 in revised MS).

Referee 2

Comments: This paper reports on the hexamethylenetetramine-mediated $CH_3NH_3PbI_3$ perovskite solar cells showing high efficiency and higher stability. This revised version paper mention the detail of the effect of hexamethyelenetetramine by XRD, photoluminescence spectra and photovoltaic performances. I think this paper meets requirements for the publication in this journal as it is.

Response: We thank for the appreciation of the Referee 2.

Graphical Abstract

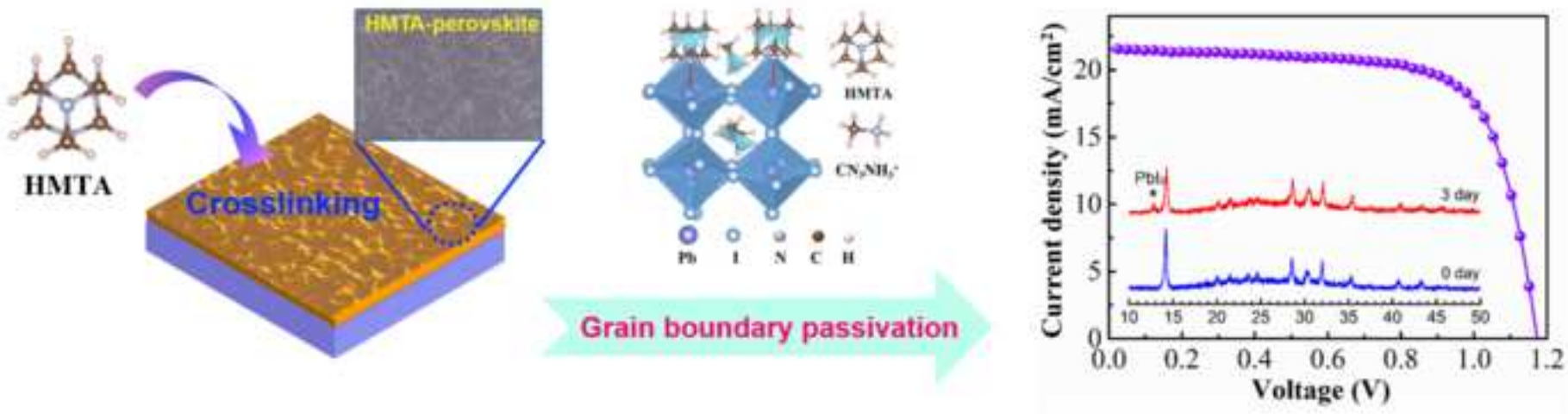

Highlights

- HMTA-assisted growth of grain boundary-passivation perovskite film is developed.
- A successive-grain-splice and PbI_2-free perovskite film is formed.
- The moisture resistance of the HMTA-mediated grown film is improved.
- Conversion efficiency achieves an average of 16.93% and a champion of 17.87%.

Hexamethylenetetramine-mediated growth of grain-boundary-passivation $CH_3NH_3PbI_3$ for highly reproducible and stable perovskite solar cells

Yan-Zhen Zheng [a,b,*], Xi-Tao Li [a], Er-Fei Zhao [a], Xin-Ding Lv [a], Fan-Li Meng [a], Chao Peng [c], Xue-Sen Lai [a], Meilan Huang [c,*], Guozhong Cao [d], Xia Tao [a,*] and Jian-Feng Chen[b]

[a] State Key Laboratory of Organic-Inorganic Composites, Beijing University of Chemical Technology, 15 Beisanhuan East Road, Beijing, 100029, P. R. China

[b] Research Center of the Ministry of Education for High Gravity Engineering & Technology, Beijing University of Chemical Technology, 15 Beisanhuan East Road, Beijing, 100029, P. R. China

[c] School of Chemistry & Chemical Engineering, Queen's University Belfast, United Kingdom

[d] Department of Materials Science and Engineering, University of Washington, Seattle, WA 98195, United States

* Corresponding author. Tel: +86-10-6445-3680 Fax: +86-10-6443-4784

E-mail: zhengyz@mail.buct.edu.cn (Y.-Z. Z.); taoxia@yahoo.com (X. T.)

Abstract

Simultaneously achieving the long-term device stability and reproducibility has proven challenging in perovskite solar cells because solution-processing produced perovskite film with grain boundary is sensitive to moisture. Herein, we develop a hexamethylenetetramine (HMTA)-mediated one-step solution-processing deposition strategy that leads to the formation of high-purity and grain-boundary-passivation $CH_3NH_3PbI_3$ film and thereby advances cell optoelectronic performance. Through morphological and structural characterizations and theoretical calculations, we demonstrate that HMTA fully occupies the moisture-exposed surface to build a bridge across grain boundary and coordinates with Pb ions to inhibit the formation of detrimental PbI_2. Such HMTA-mediated grown $CH_3NH_3PbI_3$ films achieves a decent augmentation of power conversion efficiency (PCE) from 12.70% to 17.87%. A full coverage of PbI_2-free $CH_3NH_3PbI_3$ surface on ZnO also boosts the device's stability and reproducibility.

Keywords: Perovskite solar cell; Hexamethylenetetramine; Grain-boundary-passivation; Stability; DFT calculation

Introduction

Hybrid organic-inorganic perovskite materials, such as methylammonium lead triiodide $CH_3NH_3PbI_3$, are emerging as new generation promising solar cell absorbers owing to their superior physical properties, such as excellent optical absorption capability, low binding energy of photoexcited electron-hole pairs, balanced charge transport behaviour together with extremely long diffusion length [1-5]. Perovskite layer forms between the n-type oxide (*i.e.* TiO_2, ZnO, SnO_2) and hole transport layer, followed by assembling into a photovoltaic device with mesostructure or planar heterojunction structure [6-10]. A respectable power conversion efficiency (PCE) exceeding 20% for planar solar cell has been achieved [11,12]. Control on the perovskite architecture including crystal grain size, grain boundary and crystallinity is critically vital in the fabrication of high-performance perovskite solar cells (PSCs) [5, 13-15]. The commonly used solution-processing perovskite thin film is often characteristic of large $CH_3NH_3PbI_3$ grains with numerous ionic defects (*e.g.* halide or CH_3NH_3I) and grain boundaries [16,17]. Indeed, the grain boundaries between neighbouring $CH_3NH_3PbI_3$ grains are unstable and highly sensitive to moisture, thus accelerating the perovskite degradation under ambient conditions and consequent re-formation of PbI_2 attributing to the loss of CH_3NH_3I [18]. Additionally, the charge recombination at grain boundaries is recorded to be faster than that on grains [19]. Therefore, the existence of grain boundary within the perovskite layer would inevitably cause charge recombination and consequently the degradation of cell performance. A successful example on controlling grain boundary of large perovskite grain-based film has been reported by crosslinking individual perovskite grains with the aid of butylphosphonic acid 4-ammonium chloride, leading to an improved stability of the mesoporous architecture pervoskite device [18]. From this, it can be deduced that the introduction of such molecularly engineered crosslinking agents might offer a new route for fabricating grain-boundary-modified perovskite films for high-performance planar PSC.

Back to the second problem mentioned above, we found that the existence of grain boundary within the perovskite layer would inevitably cause charge recombination and consequently the degradation of cell performance. Constructing one-dimensional (1D) nanostructures by offering a direct pathway for rapid carrier transfer in fact has been proved to be valid in dye-sensitized solar cell and mesoporous architecture PSCs as well as photocatalysis [20-26]. Thus, if intentionally constructing a 1D nanostructure within the perovskite film for planar PSCs, we presume that such a highway-like architecture would facilitate the charge transport and consequently inhibit the charge recombination. However, such a 1D highway-like perovskite architecture design in a flat substrate is difficult to be achieved without the support of a scaffold and has yet to be reported so far. Reduction of the perovskite dimensionality is believed to be able to accelerate the electron transport by embedding $CH_3NH_3PbI_3$ into ZnO nanorod scaffold, which has been verified in mesostructured PSCs [23]. Inspired by this, here an adventurous attempt to construct 1D-like framework within perovskite film is proposed.

A tertiary amine hexamethylenetetramine ($(CH_2)_6N_4$, HMTA), is usually used as template solvent to assemble new ligand-metal-ligand-type supramolecular architectures and fabricate 1D structured metal oxide, in which the lone-pair electrons on nitrogen can coordinate the empty orbits of metal ions, generating metal-ammonium complexes [27,28]. A view of anhydrous HMTA body centred lattice of the crystalline anhydrate (Fig. 1a and Fig. S1), shows three weak N···H–C intermolecular interactions between HMTA molecules in the crystal [29]. Introducing HMTA additive to control perovskite crystallization process and modify the oxide substrate brings out threefold potential advantages. First, HMTA can coordinate Pb ions on the perovskite surface, facilitating disappearance of PbI_2 and formation of pure perovskite nanocrystals [28]. Second, HMTA can also serve as nucleation-control reagent, facilitating perovskite to form an aligned orientation. Third, HMTA can cover at the

ZnO thin film to enhance the adhesion of perovskite with the oxide substrate. As such, we are motivated to develop a strategy involving the tricky perovskite crystallization design and interfacial engineering with the aid of HMTA to produce the desirable effects on cell performance by orderly arranging perovskite grains and coordinating Pb ions within perovskite.

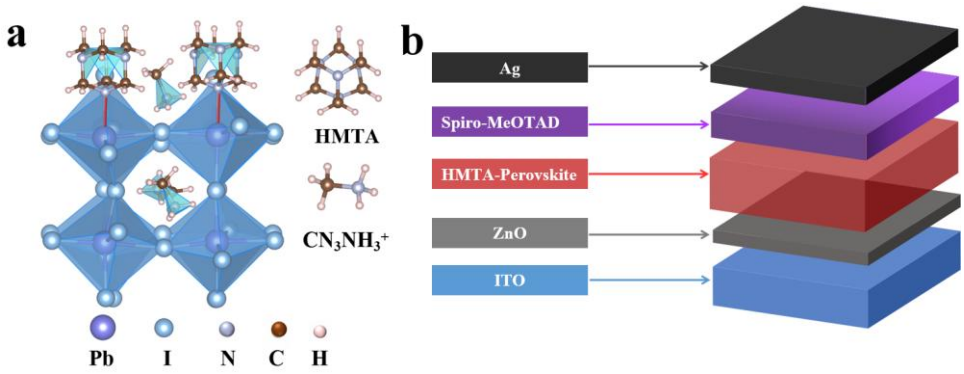

Fig. 1. (a) Schematic illustration of HMTA-assisted grown $CH_3NH_3PbI_3$ neighboring grain structure, in which HMTA coordinates Pb ion on the perovskite surface, as a result leading to orienting of neighboring perovskite grains. (b) Schematic illustration of the planar–structured perovskite solar cell configuration, where a dense and homogeneous perovskite capping layer fully covered onto the HMTA modified ZnO thin electron transport layer.

Based on the above research background, a grain boundary-passivation perovskite film was subtly prepared via a simple one-step spin-coating process mediated by HMTA to achieve high-performance PSCs. The schematic device architecture of a planar PSC with a HMTA-mediated perovskite layer is shown in Fig. 1b. Trifunctional anhydrous HMTA is used to mediate the perovskite crystallization and grain morphology and simultaneously remove the impurity PbI_2 via a simple one-step spin-coating processing method. As illustrated in Fig. 1, we find that HMTA additives pack on the perovskite surface, preventing the release of PbI_2 and therefore the potential perovskite degradation. Additionally, the perovskite surface fully covered by HMTA is modified by forming a stable insulation layer to bridge across the

grain boundary. Owing to these beneficial advantages of HMTA, a decent augmentation of PCE from 12.70% to 17.87% is achieved. Simultaneously, the reproducibility and stability of the cell are also improved in the grain-boundary-passivation, 1D-like architecture.

Results and Discussion

Perovskite films were deposited on a ZnO nanocrystal-based substrates using spin-coating a DMF solution of PbI_2, CH_3NH_3I and a small portion of HMTA via chlorobenzene-induced fast deposition crystallization (FDC) method [30]. The schematic illustration of the HMTA-assisted FDC and conventional FDC processes for fabricating perovskite film (denoted as HMTA-perovskite and pristine perovskite, respectively) are displayed in Fig. S2 and Methods in the Supporting Information. The only difference between these two FDC processes lies in whether the perovskite precursor composition contains HMTA or not. For revealing the effect of adding HMTA on the perovskite crystallization and morphology together with photovoltaic performance, various amounts of HMT additive (1.0 mg/mL, 1.5 mg/mL and 2.0 mg/mL) were introduced into perovskite precursor. X-ray diffraction (XRD) patterns of $CH_3NH_3PbI_3$/ZnO film with or without HMTA were characterized to further investigate the effect of HMTA on the nature of perovskite, as shown in Fig. 2 and Fig. S3. The diffraction peaks at 14.20^o, 28.60^o, 32.02^o, and 43.27^o are well assigned to (110), (220), (310) and (330) lattice planes of a tetragonal perovskite structure, in accordance with the $CH_3NH_3PbI_3$ reported previously [18,30]. Furthermore, for pristine perovskite film, a diffraction peak at 12.71° is clearly observed, which is ascribed to the (001) diffraction of crystallized PbI_2. The existence of PbI_2 is reported to be resulting from the humidity-induced partial decomposition of $CH_3NH_3PbI_3$ during the XRD measurement [31]. The excessive amount of PbI_2 in $CH_3NH_3PbI_3$ perovskite is harmful to the cell photovoltaic performance owing to its electrical insulating property. Additionally, the variable ratio between PbI_2 and CH_3NH_3I from batch to

batch is detrimental to the device's reproducibility. Surprisingly, no PbI_2 peak can be found by the HMTA-perovskite film, indicating a high level of phase purity and enhanced moisture resistance in the presence of the HMTA additive. From these XRD patterns, we suggest that adding HMTA in the precursor solution is able to effectively inhibit the formation of PbI_2 within perovskite film.

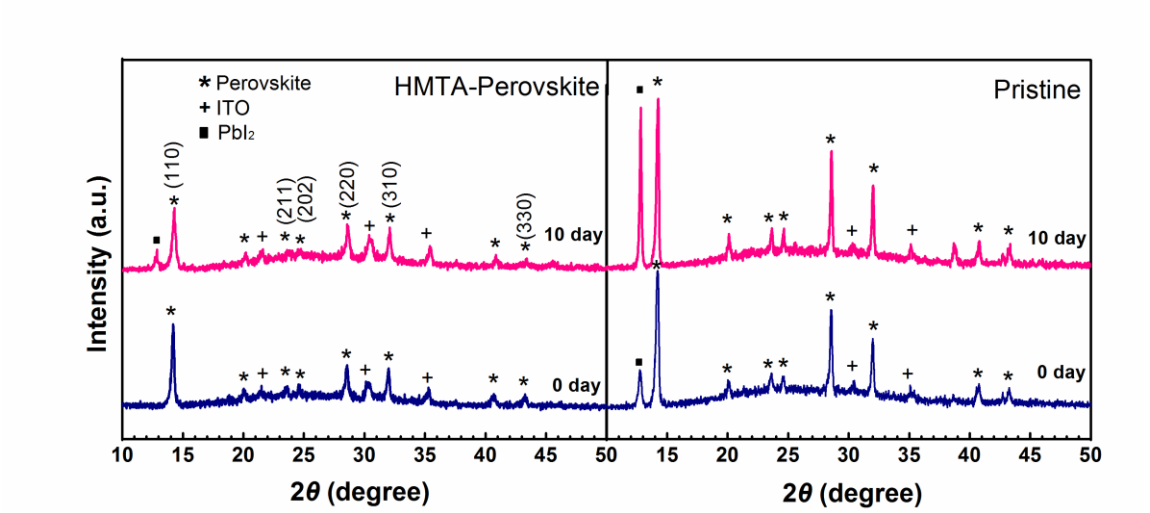

Fig. 2. XRD patterns of pristine and HMTA (1.5 mg/mL)-assisted grown $CH_3NH_3PbI_3$ films deposited on ZnO/ITO substrates before and after degradation, which are exposed to ambient air with relative humidity of 55%.

The pristine perovskite film exhibits full surface coverage stacking with perovskite grains arranging from 50 nm to 300 nm (Fig. 3a), along with observable grain boundaries between neighbouring $CH_3NH_3PbI_3$ particles over the entire perovskite capping layer. Note that such surface morphology (*e.g.* grain size) is different from previous observations [30], which is attributed to a lower perovskite precursor concentration (35wt.%) used in this work than that in published literature (45 wt.%). Strikingly, after a small amount of HMT (1.0 mg/mL) is introduced to the precursor, a part of perovskite grains starts to stack in line (Fig. S4a). Furthermore, a larger amount of HMT additive (1.5 mg/mL or 2.0 mg/mL) yields to an inter-contacting 1D-like morphology of perovskite capping layer over the ZnO film by the

aligned orientation of the perovskite grains (see Fig. 3b and Fig. S4b). Such a morphology evolution of the perovskite film is speculated attributable to the mediated perovskite crystallization process, in which anhydrous HMT fully covers the $CH_3NH_3PbI_3$ surface to build a bridge across grain boundary and hence form an inter-contacting morphology in the perovskite capping layer. Seen from Fourier transform infrared spectroscopy (FTIR) spectra of HMTA-perovskite (Fig. S5), a new adsorption band at 403 cm^{-1} associated with the Pb-N stretching [32] together with two adsorption bands at 670 cm^{-1} and 1020 cm^{-1} associated with the stretching vibrations of the C-N groups in HMTA appear, and simultaneously a band around 570 cm^{-1} corresponding to the Pb-I stretching disappears in the HMTA-perovskite, suggesting that HMTA is successfully involved in the perovskite crystallization. XPS core level peaks of Pb 4f and N1s of the perovskite and HMTA-perovskite are also given in Fig. 3c&d. Both Pb4f and N1s core signals of HMTA-perovskite shift slightly towards the higher BE (0.2 eV), indicating the coordination of nitrogen atom of the HMTA molecules with Pb ions on the perovskite surface HMTA-perovskite. In order to improve the adhesion between ZnO layer and $CH_3NH_3PbI_3$, HMTA is also introduced to modify the ZnO substrate via simply adding HMTA into ZnO precursor solution. Ultraviolet photo-electron spectroscopy (UPS) shows that the work function of ZnO is appreciably lowered from 3.84 to 3.43 eV with addition of HMTA, which is more compatible with the $CH_3NH_3PbI_3$ CBM (-3.75 eV) (see Fig. 3e). The lowered work function caused by HMTA improves the energy level alignment and electronic coupling between the ZnO and perovskite and hence increases the carrier extraction and charge generation. Moreover, the lowered ZnO work function offers a larger built-in potential for facile charge transport, thereby leading to an increase in V_{oc} of PSC.

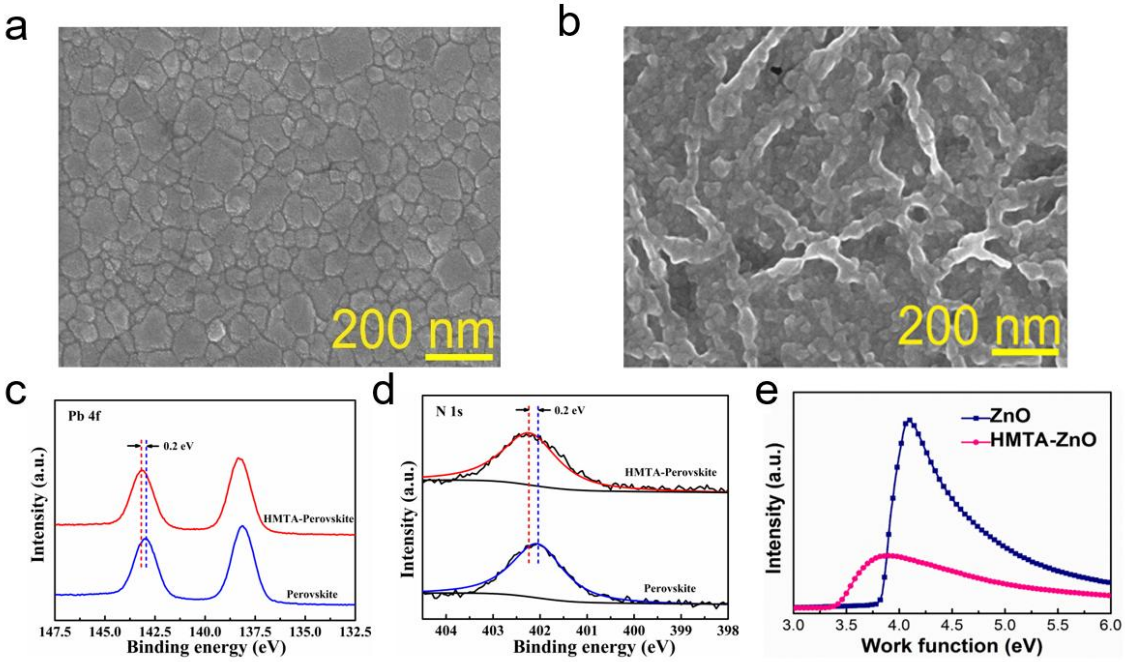

Fig. 3. SEM images of a pristine $CH_3NH_3PbI_3$ (a) and HMTA-assisted grown $CH_3NH_3PbI_3$ (b) films deposited on ZnO/ITO substrates by one-step spin-coating of the corresponding perovskite precursor solutions without or with HMTA additive. (c&d) XPS core level peaks of Pb 4f and N1s of the perovskite and HMTA-perovskite. (e) UPS of bare ZnO and HMTA-ZnO films.

Fig. 4a shows SEM images of the cross-sectional full solar cell with a configuration of ITO/HMTA-ZnO/HMTA-$CH_3NH_3PbI_3$/spiro-MeOTAD/Ag. Highly dense HMTA-$CH_3NH_3PbI_3$ film with a thickness of 250 nm is constructed on the HMTA-ZnO film with the thickness of 20 nm. The spiro-MeOTAD layer is 150 nm in thickness, adjacent to a layer of Ag with 70 nm thickness. To explore the effect of HMTA additive on device performance, PSCs based on pristine perovskite, HMTA-perovskite as well as HMTA-perovskite/HMTA-ZnO were assembled into a device architecture of ITO/compact ZnO/perovskite/spiro-OMeTAD/Ag and their photovoltaic performance were investigated. The photovoltaic parameters including short current density (J_{sc}), open-circuit voltage (V_{oc}), filled factor (*ff*) as

well as PCE best are measured under AM 1.5 G full solar illumination under reverse and forward scan directions (Fig. 4b & Fig. S6) and given in Table 1. The pristine cell shows a PCE of 12.70%, with a J_{sc} of 18.50 mA cm^{-2}, a V_{oc} of 1.09 V, and a *ff* of 0.63 respectively under reverse scan direction. However, the PCE slightly drops to 9.64% under forward scan direction, indicating a serious device hysteresis. The device performance is improved when HMTA (1.0 ~ 2.5 mg/mL) is added in the perovskite crystalline growth, with the maximum PCEs of 14.92% and 12.99% for the 1.5 mg/mL HMTA-based cell under the reverse and forward scan directions, respectively (Fig. S6&S7 and Table 1). Further improvement in the photovoltaic performance is achieved by means of HMTA-modified ZnO electron transport layer to endow a more compact and higher coverage of perovskite capping layer. Consequently, the HMTA-perovskite/HMTA-ZnO-based cell exhibits a highest PCE of 17.87% among the fabricated devices involving in this work, with a J_{sc} of 21.51 mA cm^{-2}, a V_{oc} of 1.17 V, and a *ff* of 0.71 under reverse scan condition, respectively. A PCE of 16.94% is achieved under forward scan direction, indicating a lower *J*-*V* hysteresis for the HMTA-perovskite/HMTA-ZnO-based cell as compared to the former two devices. Fig. 4c-f show the static histogram of the device parameters for all of the independently fabricated cells. All the devices assembled with HMTA-perovskite/HMTA-ZnO exhibit an overall efficiency exceeding of 16% under standard simulated solar radiation (See Table S1), suggesting that HMTA additive facilitates forming a highly reproducible $CH_3NH_3PbI_3$ capping layer and PSC by simultaneously controlling perovskite crystallization and improving the interface between perovskite and oxide substrate. Moreover, the HMTA-perovskite/HMTA-ZnO-based PSC exhibits photovoltaic parameters with small standard deviation, leading to an average PCE of 16.93±0.43%, with J_{sc} of 21.33±0.44 mA cm^{-2}, V_{oc} of 1.16±0.02 V, and *ff* of 0.69±0.02. The average PCE (16.93±0.43%) of HMTA-perovskite/HMTA-ZnO-based PSC is much higher than that of pristine perovskite/ZnO based- (11.65±0.67%) (Table S2), and HMTA-

perovskite/ZnO-based PSCs (14.21±0.49%) (Table S3), indicating a significantly improved reproducibility for the HMTA-perovskite/HMTA-ZnO-based PSC.

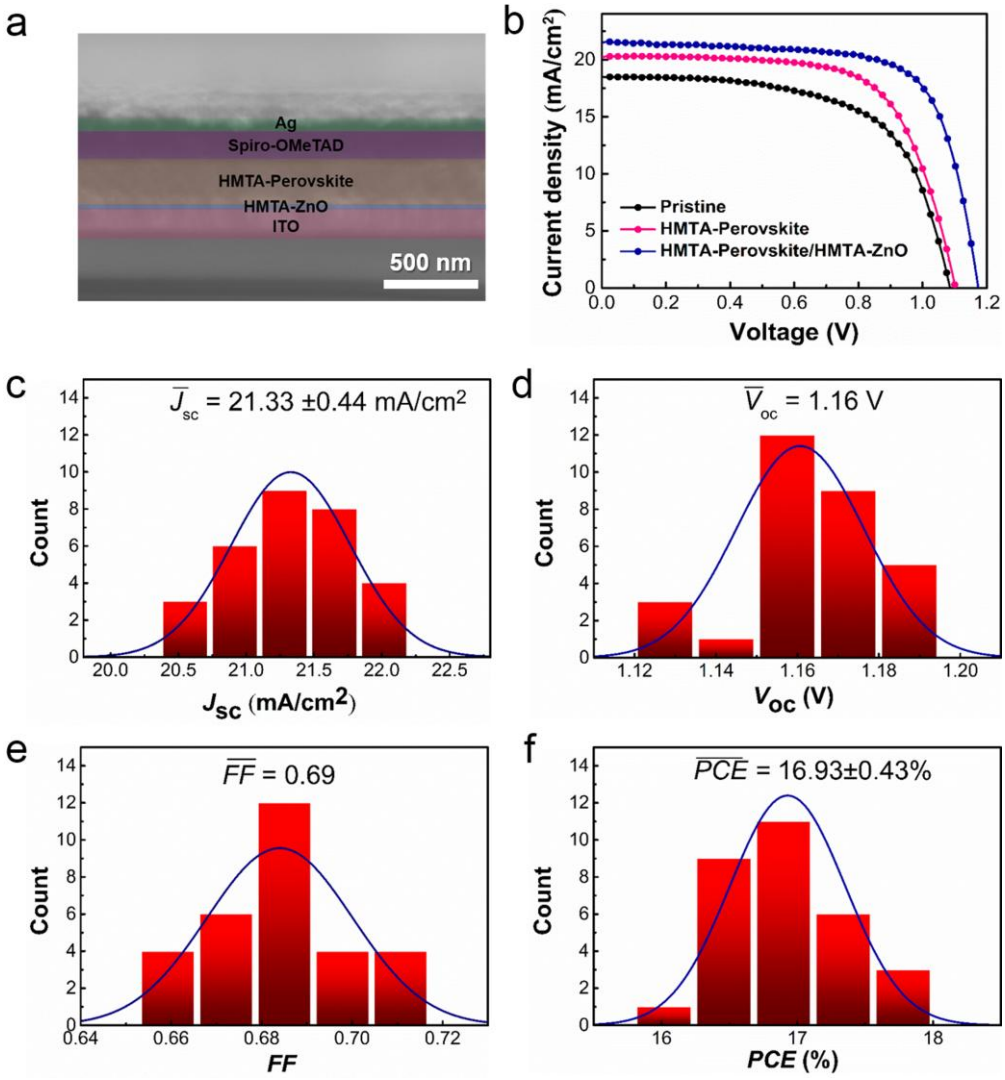

Fig. 4. (a) Cross-sectional SEM image of an optimized device, in which the thickness of HMTA-ZnO, $CH_3NH_3PbI_3$, spiro-MeOTAD, and Ag are 20, 250, 150, and 70 nm, respectively. (b) *J-V* curves measured under AM 1.5 simulated sunlight for the best performing PSCs based on pristine perovskite, HMTA-perovskite, and HMTA-perovskite/HMTA-ZnO films, respectively. (c-f) Histograms of V_{oc}, J_{sc}, *FF*, and *PCE* of 30 cells based on HMTA-perovskite/HMTA-ZnO film, respectively.

Table 1 Photovoltaic parameters of PSCs based on pristine perovskite, HMTA-perovskite, and HMTA-perovskite/HMTA-ZnO films under reverse and forward scan directions.

Cells	Scan directions	V_{oc} (V)	J_{sc} (mA cm^{-2})	*FF*	*PCE* (%)
Pristine	Reverse	1.09	18.50	0.63	12.70
	Forward	1.00	17.48	0.55	9.64
HMTA-Perovskite	Reverse	1.10	20.24	0.67	14.92
	Forward	1.08	19.73	0.61	12.99
HMTA-Perovskite/HMTA-ZnO	Reverse	1.17	21.51	0.71	17.87
	Forward	1.17	21.29	0.68	16.94

$CH_3NH_3PbI_3$ is sensitive to moisture due to its ionic character, and the performance of the PSCs degrades rapidly in a humid environment [33-35]. Thus, the long-term device stability of pristine perovskite-ZnO and HMTA-perovskite/HMTA-ZnO under atmospheric conditions at room temperature are also investigated. First, the pristine and HMTA-perovskite films deposited on ZnO/ITO substrates are continuously exposed to ambient air with relative humidity of 55% at room temperature for 10 days. The perovskite degradation is traced by recording the corresponding perovskite film XRD pattern at the beginning and end of the periods. For the pristine perovskite, the intensity of the characteristic PbI_2 (001) peak at 12.65^o becomes much stronger after 10 days (Fig. 2), indicating that the pristine perovskite contains large amounts of PbI_2 and is severely corroded by moisture upon being exposed under ambient air [36,37]. In contrast, after exposed to ambient air for 10 days a very weak PbI_2 peak is discerned for the aged HMTA-perovskite film, implying a much lower degree of decomposition compared with the pristine perovskite. This means HMTA additives prevent the perovskite from humidity. The time evolutions of the photovoltaic parameters including V_{oc}, J_{sc}, *ff*, and PCE of the both unencapsulated PSCs are recorded and shown in Fig. 5a&b. The PCE increases in the initial stage of the aging test with a highest value obtained while the unencapsulated HMTA-perovskite/HMTA-ZnO cell is aged for 24 h, and then only gently

decreases during the period of 24~720 h, with retention of 53% of its highest value within 720 h. By contrast, the J_{sc}, and *ff* values for the pristine PSC suffer a substantial decrease during the aging period, leading to a normalized PCE decay to 12% of its highest value within 720 h. Moreover, to ensure the accuracy of our measurement, the photovoltaic performance stability of a batch of 30 unencapsulated HMTA-perovskite/HMTA-ZnO and pristine perovskite devices are measured, and the corresponding statistical results are also shown in Fig 5c&d. Error bars represent the standard deviation of the measured PCE for the HMTA-perovskite/HMTA-ZnO and pristine perovskite PSCs (30 devices). Statistical results from thirty individual HMTA-perovskite/HMTA-ZnO and pristine perovskite devices show a reliable fabrication of the HMTA-perovskite based planar PSC device with better electrical stability. A tiny change in the XRD patterns and a smaller reduce in photovoltaic performance within the aging period demonstrate that the morphology evolution and interface modification of the perovskite film by HMTA prevent H_2O from accessing perovskite, and therefore block the CH_3NH_3I extraction and inhibit the formation of PbI_2. The improved moisture resistance of the HMTA-mediated grown film growth is likely to originate from the shielding effect of the final compact and grain-boundary-passivation perovskite films that protects the inner perovskite grains from moisture and thus attenuates the degradation process. The improved average efficiency, reproducibility and stability verify the influence of HMTA additive on the composition of the perovskite layer and the interface optimization of the cell device. The comprehensive comparison of perovskite structure and photovoltaic performance between HMTA-perovskite and other reported similar materials modified PSCs is shown in Table S4 [18, 37, 38]. It is evident that the PCE of the HMTA-perovskite based planar PSC is superior to those of any other modifiers to date, owing to the dual-functional HMTA to synchronously mediate perovskite crystallization and modify the interface between ZnO and perovskite. More importantly, HMTA-perovskite precursor enables a simple one-step spin-coating deposition of a uniform and fully covered PbI_2-free perovskite layer. It is worth pointing out

that the stability of the $CH_3NH_3PbI_3$ perovskite-based ZnO PSC is rarely reported owing to the remaining hydroxyl groups and/or residual acetate ligands on the ZnO surface accelerating the decomposition of $CH_3NH_3PbI_3$. In this work, we have demonstrated the stability of $CH_3NH_3PbI_3$-based ZnO PSC with HMTA additive is improved, as shown in updated Fig. 2 and Fig. 5. Thus, taking account of its superiority in the PCE and feasibility of simple processing fully covered PbI_2-free perovskite film together with modifying ZnO-perovskite interface, HMTA is a promising additive for high performance PSCs with improved stability.

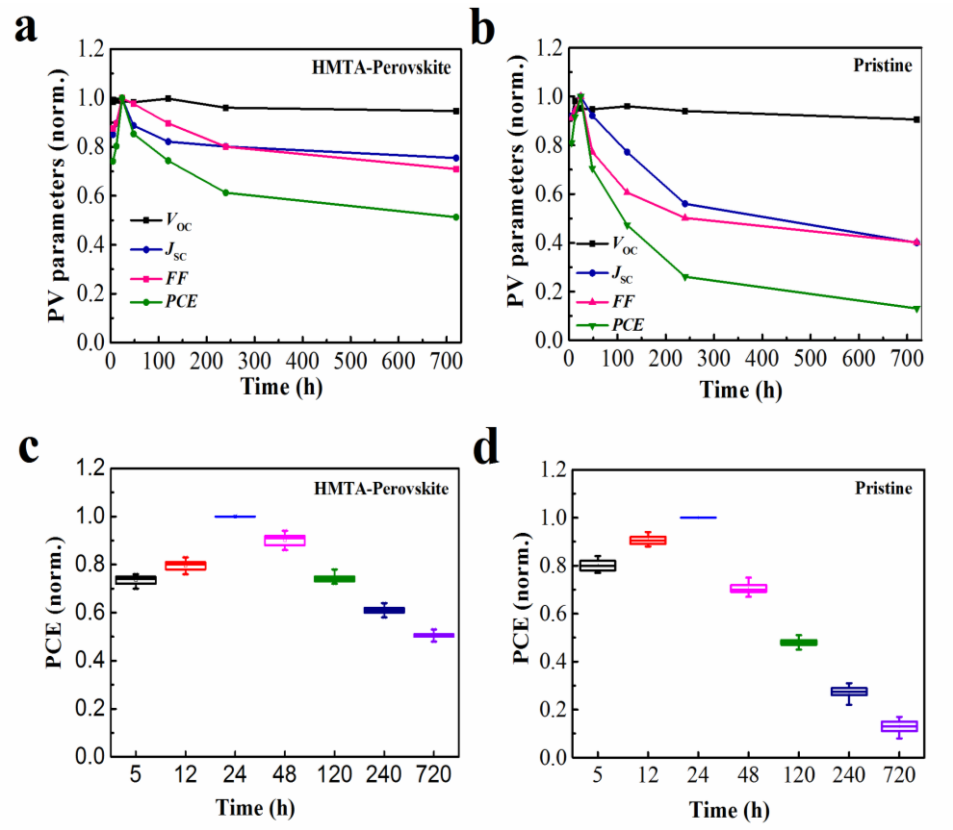

Fig. 5. Evolution of normalized device photovoltaic parameters of the unsealed PSCs based on HMTA- perovskite/HMTA-ZnO films (a), and pristine perovskite (b) that are stored in ambient air at ~55% humidity in the dark. Error bars represent the standard deviation of the measured PCE for the HMTA- perovskite/HMTA-ZnO (c), and pristine perovskite (d) PSCs (30 devices).

We perform DFT calculations on the adsorption of the HMTA molecules at two stoichiometric tetragonal $CH_3NH_3PbI_3$ surfaces, namely the (110) and (100) surfaces (Fig. S8), in order to understand the molecular mechanism for improved PSC performance. It can be found that HMTA can occupy at the penta-coordinated Pb site with favorable adsorption energies on both $CH_3NH_3PbI_3$ surfaces (Table S5), forming a compactly packed layer (Fig. 6). This is in accordance with the boundary-free PSC grain observed in our SEM experiments. Moreover, the strong Pb-HMTA coordination and the compactly packed perovskite block the formation of PbI_2, thus preventing the possible degradation of PSCs. Interestingly, the surficial Pb-I bond is partially distorted with single HMTA adsorbed at the (100) surface but is restored in the fully covered surface (Fig. S9), which accounts for the much higher adsorption energy and stability of the surface with high coverage. The adsorption of HMTA at the surficial $CH_3NH_3^+$ (MA^+) vacancies (Fig. S10) was also investigated. We find that the strong Pb-N bond observed in the adsorption of HMTA at the Pb site is replaced by the weak hydrogen bond interaction formed between the tetramine H and I atoms, demonstrating HMTA may adsorb at both the Pb and MA^+ sites. On the other hand, when the HMTA molecules fully occupy the active site of the Pb cations, the modified surfaces may sterically hinder H_2O molecules from accessing the Pb ions and adsorbing on the surfaces. Competitive adsorption of H_2O on the surface was considered in order to determine predominant adsorption under ambient conditions. We find that the adsorption energies of H_2O molecules at the Pb sites are lower than those of the HMTA additive (Table S5, Fig. S11). In particular, the adsorption of H_2O with high coverage at the surficial MA^+ vacancies is much unfavourable than HMTA, indicating the surface is inclined to be covered by the HMTA additive rather than by H_2O. This is in accordance with our XRD observations that the HMTA-perovskites exhibit moisture stability under ambient conditions. In view of the features of the perovskite surfaces adsorbed with HMTA in the aspects of morphology, stability and moisture-resistance, the HMTA additives may function as an efficient nucleation

solvent to prevent the release of PbI_2 and arrange themselves on the perovskite surface to hinder the contact with water [39-43].

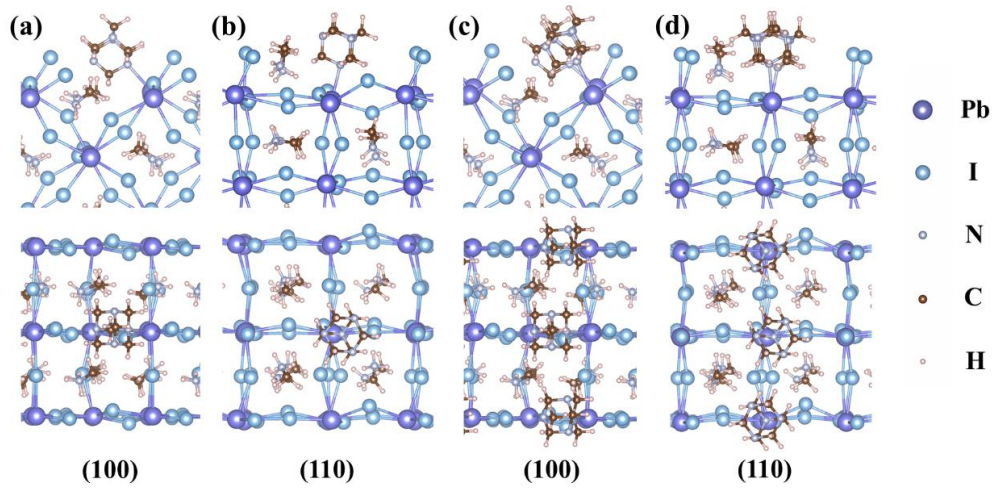

Fig. 6. DFT calculations on the adsorption of the HMTA molecules at two stoichiometric tetragonal $CH_3NH_3PbI_3$ surfaces. Top (upper panel) and side (lower panel) views of the optimized geometries of the tetragonal $CH_3NH_3PbI_3$ surfaces loaded with HMTA. (a& b) One HMTA is adsorbed on the (100) and (110) surfaces, respectively. **(**c&d) Two HMTA molecules adsorbed on the (100) and (110) surfaces, respectively. HMTA is adsorbed on the exposed Pb^{2+} site.

In a PSC, the deposition of perovskite on ZnO-based substrates, which is closely related with the sunlight absorption capacity, is another crucial factor that affects perovskite device performance. The absorption spectra of both HMTA-perovskite/ZnO-based films are only slightly lower than that of pristine perovskite film, which indicates that HMTA additive does not prompt the perovskite deposition on the ZnO substrate (Fig. S12). Besides, the absorption spectra in the regions of 400 ~ 550 nm and 700 ~ 800 nm of HMTA-perovskite/ZnO is ~ 5 nm blue shifted with respect to that of the pristine perovskite film, indicating a higher bandgap for 1D-like HMTA-perovskite/ZnO film. Such a slight shift in absorption spectra

upon introducing the HMTA additive in the perovskite crystal growth may arise from the increasing surface-to-volume ratio of the 1D-like perovskite [44].

The trap states within the perovskite surface have been proved to be related to the crystallinity and grain size as well as grain boundary of perovskite film [45]. Fig. 7 shows the steady-state photoluminescence (SS-PL) spectra of pristine perovskite/ZnO, HMTA-perovskite/ZnO, and HMTA-perovskite/HMTA-ZnO films, which are excited at 460 nm, and detected at the band edge of $CH_3NH_3PbI_3$ perovskite film (*i.e.* 775 nm). In comparison with the pristine perovskite/ZnO film, the PL intensity of the HMTA-perovskite/ZnO is significantly increased, which may result from the reduction of trap state mediated PL behaviour [4]. Thus, it can be deduced that the HMTA additive as nucleation-assisted agent is able to remarkably reduce the number of trap states owing to orienting the perovskite grains to form successive 1D-like morphology [4,12,13]. As for HMTA-perovskite/HMTA-ZnO film, the intensity is further enhanced because of the reduction of pin holes within the perovskite surface and improvement of morphology. The enhanced PL intensity of the HMTA-perovskite/ZnO or HMTA-perovskite/HMTA-ZnO film manifests the reduction of trap state defects within the perovskite at the interface, which inhibits charge recombination and hence increases exciton diffusion length, resulting in the highly efficient cell. Additionally, from Fig. 7, we can also observe that emission maxima locates at around 767 nm for pristine perovskite-ZnO film, and it centres at around 762 nm for both HMTA-perovskite/ZnO and HMTA-perovskite/HMTA-ZnO films, corresponding to an approximate 5 nm stokes shift with respect to the pristine perovskite film. Such a slight blue shift in PL spectra, which is likely originating from more localized excitons in 1D-like architecture, was also reported in nanowire perovskite film [39]. This observed phenomenon concerning emission peak shift is in consistence with the UV-vis spectra shown in Fig. S12. Thus, the HMTA-mediated solution processing for deposition of perovskite on ZnO substrate, together with HMTA interface engineering for facilitating the strong electronic coupling between perovskite and

HMTA/ZnO effectively suppress the formation of defects or trap states within perovskite crystallization and then inhibit the charge recombination, and consequently leading to a high optoelectronic conversion performance.

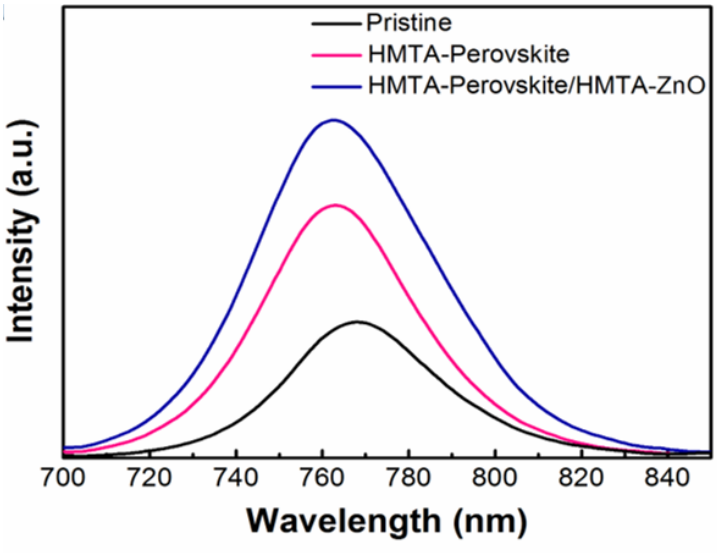

Fig. 7. SS-PL spectra of pristine perovskite, HMTA-perovskite, and HMTA-perovskite/HMTA-ZnO films on ZnO/ITO substrates, respectively.

Conclusions

To summarize, a facile one-step HMTA-mediated solution deposition method has been developed for reproducible fabrication of a high-quality 1D-like $CH_3NH_3PbI_3$ thin films, in which HMTA allows controlling over the $CH_3NH_3PbI_3$ crystallization by aligning perovskite grains and coordinating with PbI_2. XRD, SEM, FTIR and DFT calculation results demonstrate a high-purity of $CH_3NH_3PbI_3$ thin film with no PbI_2 impurity through HMTA being coordinated with Pb ions and fully occupying the $CH_3NH_3PbI_3$ surface to build a bridge across grain boundary and coordinating with Pb ions. The HMTA-assisted growth of perovskite film yields an appreciable enhancement in both photovoltaic performance, reproducibility together with stability in comparison with the pristine perovskite, leading to a PCE of 17.87%. The

simple, HMTA-mediated and low temperature solution method can be applied to construction of other perovskite-based hybrid optoelectronic devices.

Acknowledgements

The work was supported by the National Natural Science Foundation of China (Nos. 21476019, 21676017, 21377011).

Notes and references

[1] A. Kojima, K. Teshima, Y. Shirai, T. Miyasaka, J. Am. Chem. Soc., 131 (2009) 6050-6051.

[2] M. M. Lee, J. Teuscher, T. Miyasaka, T. N. Murakami, H. J. Snaith, Science, 338 (2012) 643-647.

[3] S. D. Stranks, G. E. Eperon, G. Grancini, C. Menelaou, M. J. Alcocer, T. Leijtens, L. M. Herz, A. Petrozza, H. J. Snaith, Science, 342 (2013) 341-344.

[4] G. Xing, N. Mathews, S. Sun, S. S. Lim, Y. M. Lam, M. Grätzel, S. Mhaisalkar, T. C. Sum, Science, 342 (2013) 344-347.

[5] Z. Zhao, X. Chen, H. Wu, X. Wu, G. Cao, Adv. Funct. Mater., 2016, 26, 3048-3058.

[6] Y.-Z., Zheng, E.-F. Zhao, F.-L. Meng, X.-S. Lai, X.-M. Dong, J.-J. Wu, X. Tao, J. Mater. Chem. A, 5 (2017) 12416-12425.

[7] W. Ke, G. Fang, Q. Liu, L. Xiong, P. Qin, H. Tao, J. Wang, H. Lei, B. Li, J. Wan, J. Am. Chem. Soc., 137 (2015) 6730-6733.

[8] Y. Luo, F. Meng, E. Zhao, Y.-Z. Zheng, Y. Zhou, X. Tao, J. Power Sources, 311 (2016) 130-136.

[9] D. Yang, X. Zhou, R. Yang, Z. Yang, W. Yu, X. Wang, C. Li, S. F. Liu, R. P. Chang, Energy Environ. Sci., 9 (2016) 3071-3078.

[10] M. Cha, P. Da, J. Wang, W. Wang, Z. Chen, F. Xiu, G. Zheng, Z.-S. Wang, J. Am. Chem. Soc., 138 (2016) 8581-8587.

[11] H. Tan, A. Jain, O. Voznyy, X. Lan, F. P.G. Arquer, J.Z. Fan, R. Quintero-Bermudez, M. Yuan, B. Zhang, Y. Zhao, F. Fan, P. Li, L. N. Quan, Y. Zhao, Z.-H. Lu, Z. Yang, S. Hoogland, E. H. Sargent, Science, 355 (2017) 722-726.

[12] F. Cai, L. Yang, Y. Yan, J. Zhang, F. Qin, D. Liu, Y.-B. Cheng, Y. Zhou, T. Wang, J. Mater. Chem. A, 5 (2017) 9402-9411.

[13] V. D'Innocenzo, G. Grancini, M. J. P. Alcocer, A. R. S. Kandada, S. D. Stranks, M. M. Lee, G. Lanzani, H. J. Snaith, A. Petrozza, Nat. Commun., 5 (2014) 3586.

[14] C. Wehrenfennig, M. Liu, H. J. Snaith, M. B. Johnston, L. M. Herz, Energy Environ. Sci., 7 (2014) 2269-2275.

[15] S.-S. Li, C.-H. Chang, Y.-C. Wang, C.-W. Lin, D.-Y. Wang, J.-C. Lin, C.-C. Chen, H.-S. Sheu, H.-C. Chia, W.-R. Wu, Energy Environ. Sci., 9 (2016) 1282-1289.

[16] J. Burschka, N. Pellet, S. J. Moon, R. Humphry-Baker, P. Gao, M. K. Nazeeruddin, M. Grätzel, Nature, 499 (2013) 316-319.

[17] Q. Chen, H. Zhou, T. B. Song, S. Luo, Z. Hong, H. S. Duan, L. Dou, Y. Liu, Y. Yang, Nano Lett., 14 (2014) 4158-4163.

[18] X. Li, M. I. Dar, C. Yi, J. Luo, M. Tschumi, S. M. Zakeeruddin, M. K. Nazeeruddin, H. Han, M. Grätzel, Nat. Chem., 7 (2016) 703-711.

[19] D. W. Dequilettes, S. M. Vorpahl, S. D. Stranks, H. Nagaoka, G. E. Eperon, M. E. Ziffer, H. J. Snaith, D. S. Ginger, Science, 348 (2016) 683-686.

[20] Y. Z. Zheng, J. Zhao, H. Zhang, J. F. Chen, W. Zhou, X. Tao, Chem. Commun., 47 (2011) 11519-11521.

[21] Y. Z. Zheng, H. Ding, Y. Liu, X. Tao, G. Cao, J. F. Chen, J. Power Sources, 254 (2014) 153-160.

[22] Y.-Z. Zheng, X. Tao, L.-X. Wang, H. Xu, Q. Hou, W.-L. Zhou, J.-F. Chen, Chem. Mater., 22 (2010) 928-934.

[23] D. Y. Son, J. H. Im, H. S. Kim, N. G. Park, J. Phys. Chem. C, 118 (2014) 16567-16573.

[24] X. H. Lu, Y. Z. Zheng, S. Q. Bi, Y. Wang, X. Tao, L. Dai, J. F. Chen, Adv. Energy Mater., 4 (2016) 1301802.

[25] K. Mahmood, B. S. Swain, A. Amassian, Adv. Energy Mater., 5 (2016) 1500568.

[26] Y. Wang, Y.-Z. Zheng, S. Lu, X. Tao, Y. Che, J.-F. Chen, ACS Appl. Mater. Interfaces, 7 (2015) 6093-6101.

[27] G. Durá, M. C. Carrión, F. A. Jalón, B. R. Manzano, A. M. Rodríguez, K. Mereiter, Cryst. Growth Des., 15 (2015) 3321-3331.

[28] Y. Tong, Y. Liu, L. Dong, D. Zhao, J. Zhang, Y. Lu, D. Shen, X. Fan, J. Phys. Chem. B, 110 (2006) 20263-20267.

[29] R. C. Burton, E. S. Ferrari, R. J. Davey, J. L. Finney, D. T. Bowron, J. Phys. Chem. B, 113 (2009) 5967-5977.

[30] M. Xiao, F. Huang, W. Huang, Y. Dkhissi, Y. Zhu, J. Etheridge, A. Gray-Weale, U. Bach, Y. B. Cheng, L. Spiccia, Angew. Chem., 126 (2014) 10056-10061.

[31] E. Horváth, M. Spina, Z. Szekrényes, K. Kamarás, R. Gaal, D. Gachet, L. Forró, Nano Lett., 14 (2014) 6761-6766.

[32] B. A. Uzoukwu, P. U. Adiukwu, Synth. React. Inorg. Met.-Org. Chem., 27 (1997) 187-195.

[33] M. Grätzel, Nat. Mater., 13 (2014) 838-842.

[34] A. Dualeh, P. Gao, I. S. Sang, M. K. Nazeeruddin, M. Grätzel, Chem. Mater., 26 (2014) 6160-6164.

[35] J. M. Frost, K. T. Butler, F. Brivio, C. H. Hendon, M. V. Schilfgaarde, A. Walsh, Nano Lett., 14 (2014) 2584-2590.

[36] H. A. Harms, N. Pellet, M. Bensimon, Faraday Discuss., 176 (2014) 251-269.

[37] L. Zuo, Z. Gu, T. Ye, W. Fu, G. Wu, H. Li, H. Chen, J. Am. Chem. Soc., 137 (2015) 2674-2679.

[38] J. Zhang, Z. Hu, L. Huang, G. Yue, J. Liu, X. Lu, Z. Hu, M. Shang, L. Han, Y. Zhu, Chem. Commun., 51 (2015) 7047-7050.

[39] I. C. Smith, E. T. Hoke, S. I. Diego, M. D. Mcgehee, H. I. Karunadasa, Angew. Chem. Int. Ed., 53 (2014) 11232-11235.

[40] Y. Wu, A. Islam, X. Yang, C. Qin, J. Liu, K. Zhang, W. Peng, L. Han, Energy Environ. Sci., 7 (2014) 2934-2938.

[41] H. Zhang, J. Mao, H. He, D. Zhang, H. L. Zhu, F. Xie, K. S. Wong, M. Grätzel, W. C. Choy, Adv. Energy Mater.,5 (2015) 1501354.

[42] Y.-J. Jeon, S. Lee, R. Kang, J.-E. Kim, J.-S. Yeo, S.-H. Lee, S.-S. Kim, J.-M. Yun, D.-Y. Kim, Sci. Rep., 4 (2014) 6953.

[43] S. Yang, Y. Wang, P. Liu, Y.-B. Cheng, H. J. Zhao, H. G. Yang, Nat. Energy, 1 (2016) 15016.

[44] J. H. Im, J. Luo, M. Franckevičius, N. Pellet, P. Gao, T. Moehl, S. M. Zakeeruddin, M. K. Nazeeruddin, M. Grätzel, N. G. Park, Nano Lett., 15 (2015) 2120-2126.

[45] H. Oga, A. Saeki, Y. Ogomi, S. Hayase, S. Seki, J. Am. Chem. Soc., 136 (2014) 13818-13825.

Table 1 Photovoltaic parameters of PSCs based on pristine perovskite, HMTA-perovskite, and HMTA-perovskite/HMTA-ZnO films under reverse and forward scan directions.

Cells	Scan directions	V_{oc} (V)	J_{sc} (mA cm^{-2})	*FF*	*PCE* (%)
Pristine	Reverse	1.09	18.50	0.63	12.70
	Forward	1.00	17.48	0.55	9.64
HMTA-Perovskite	Reverse	1.10	20.24	0.67	14.92
	Forward	1.08	19.73	0.61	12.99
HMTA-Perovskite/HMTA-ZnO	Reverse	1.17	21.51	0.71	17.87
	Forward	1.17	21.29	0.68	16.94

Figure 1

Click here to download high resolution image

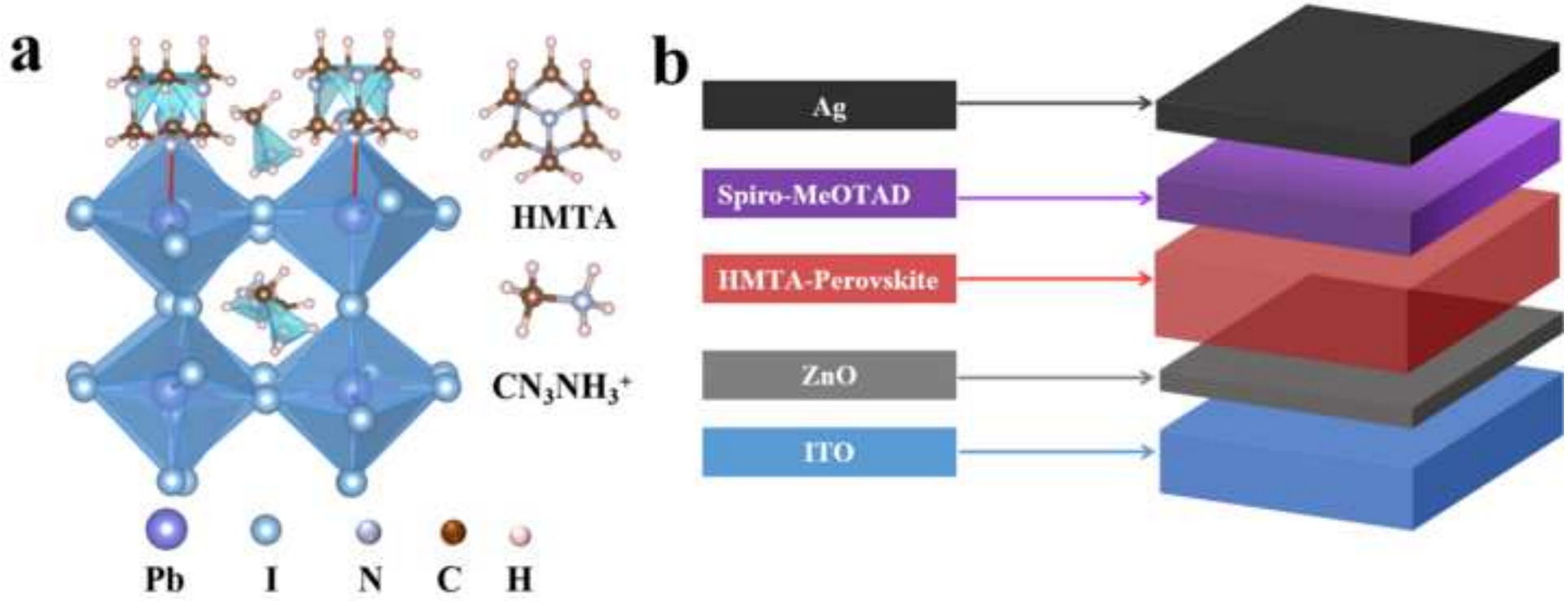

Figure 2

Click here to download high resolution image

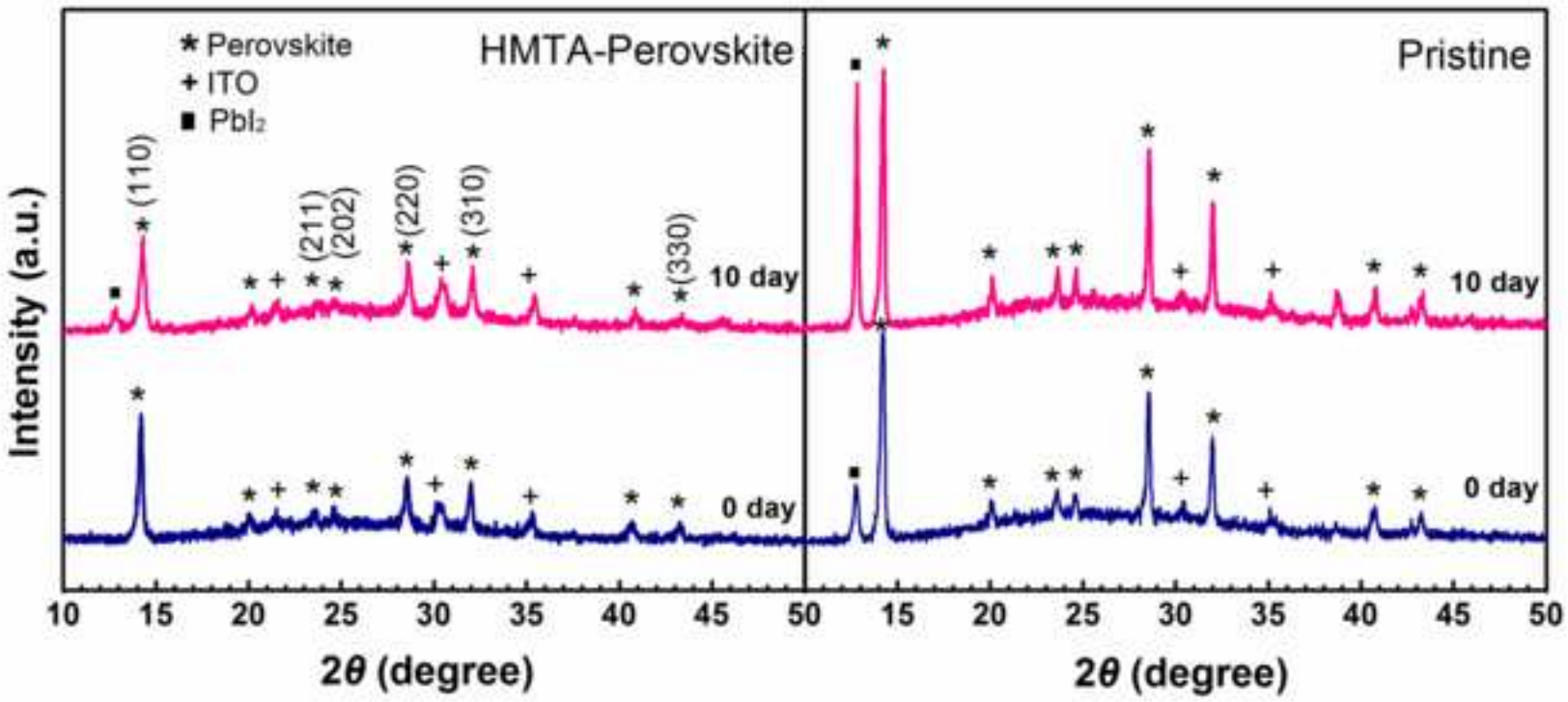

Figure 3

Click here to download high resolution image

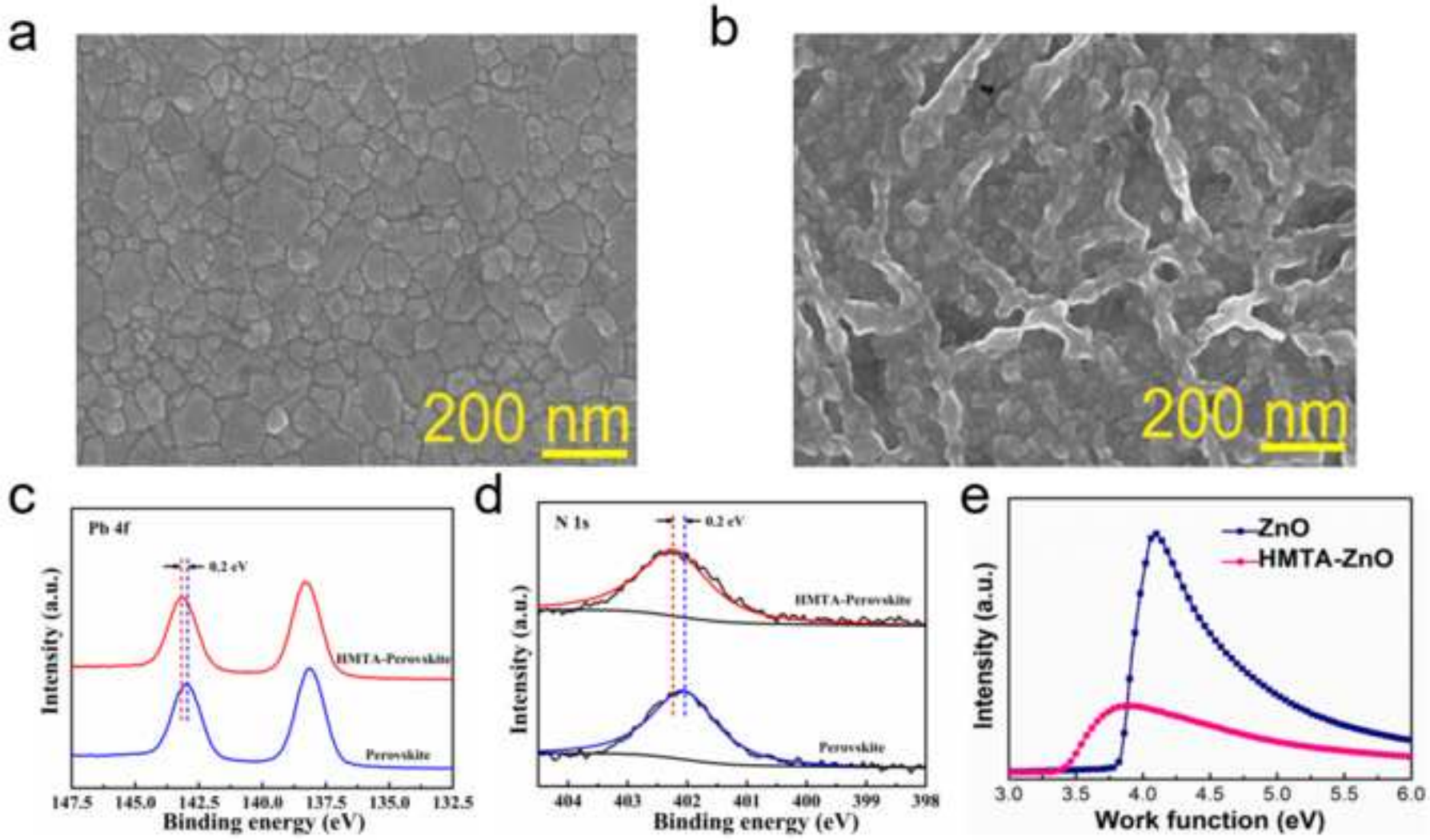

Figure 4

Click here to download high resolution image

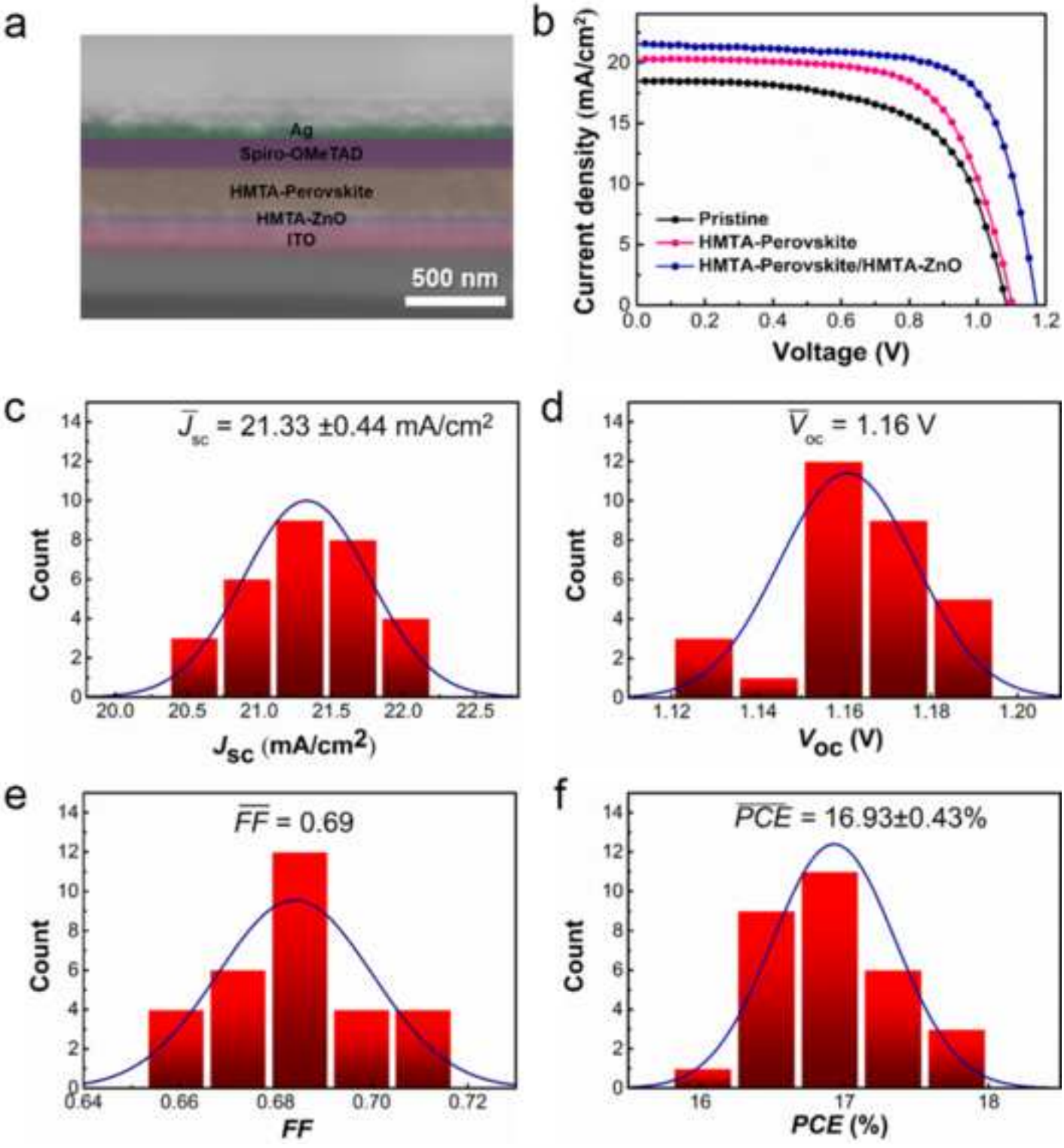

Figure 5

Click here to download high resolution image

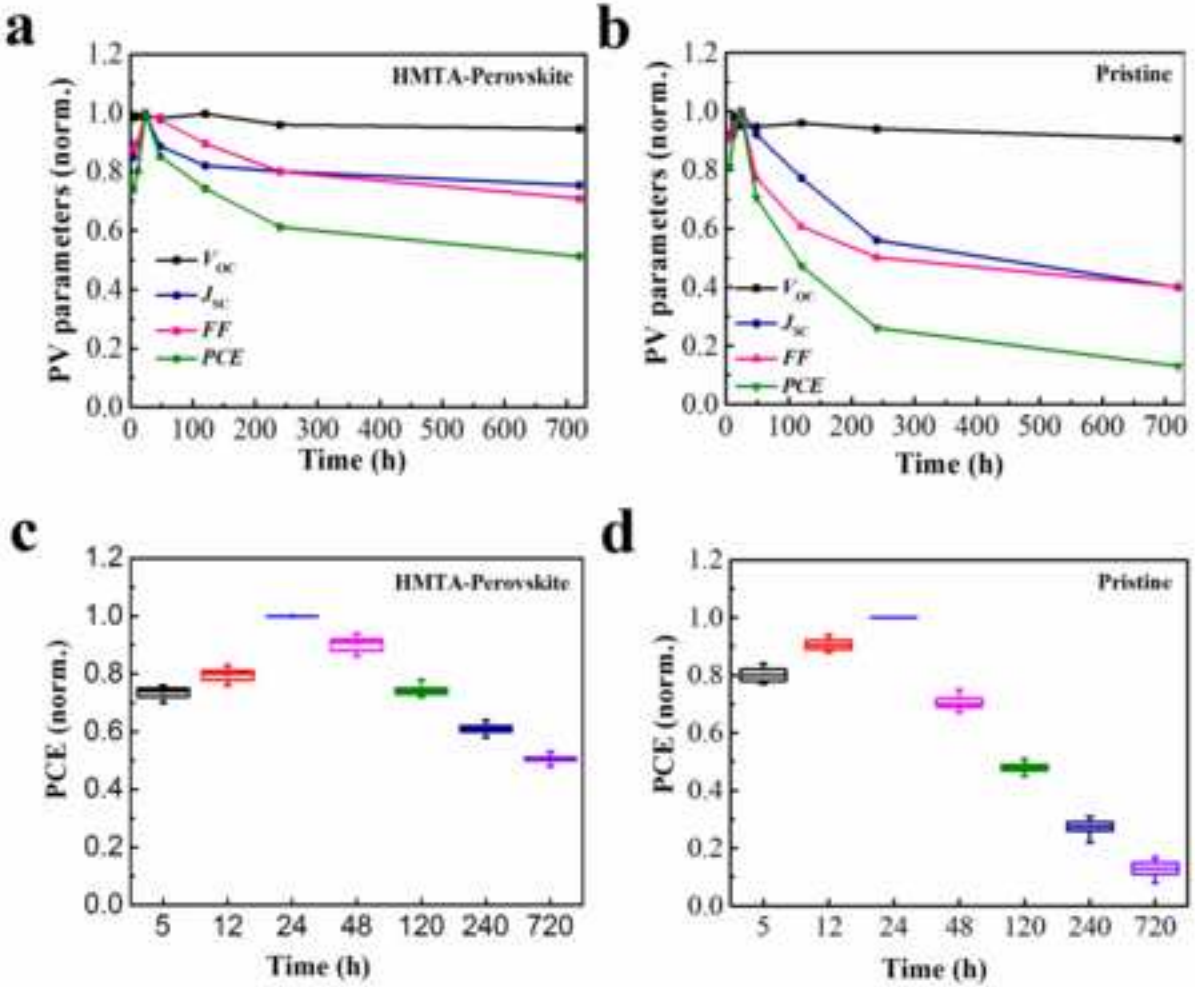

Figure 6

Click here to download high resolution image

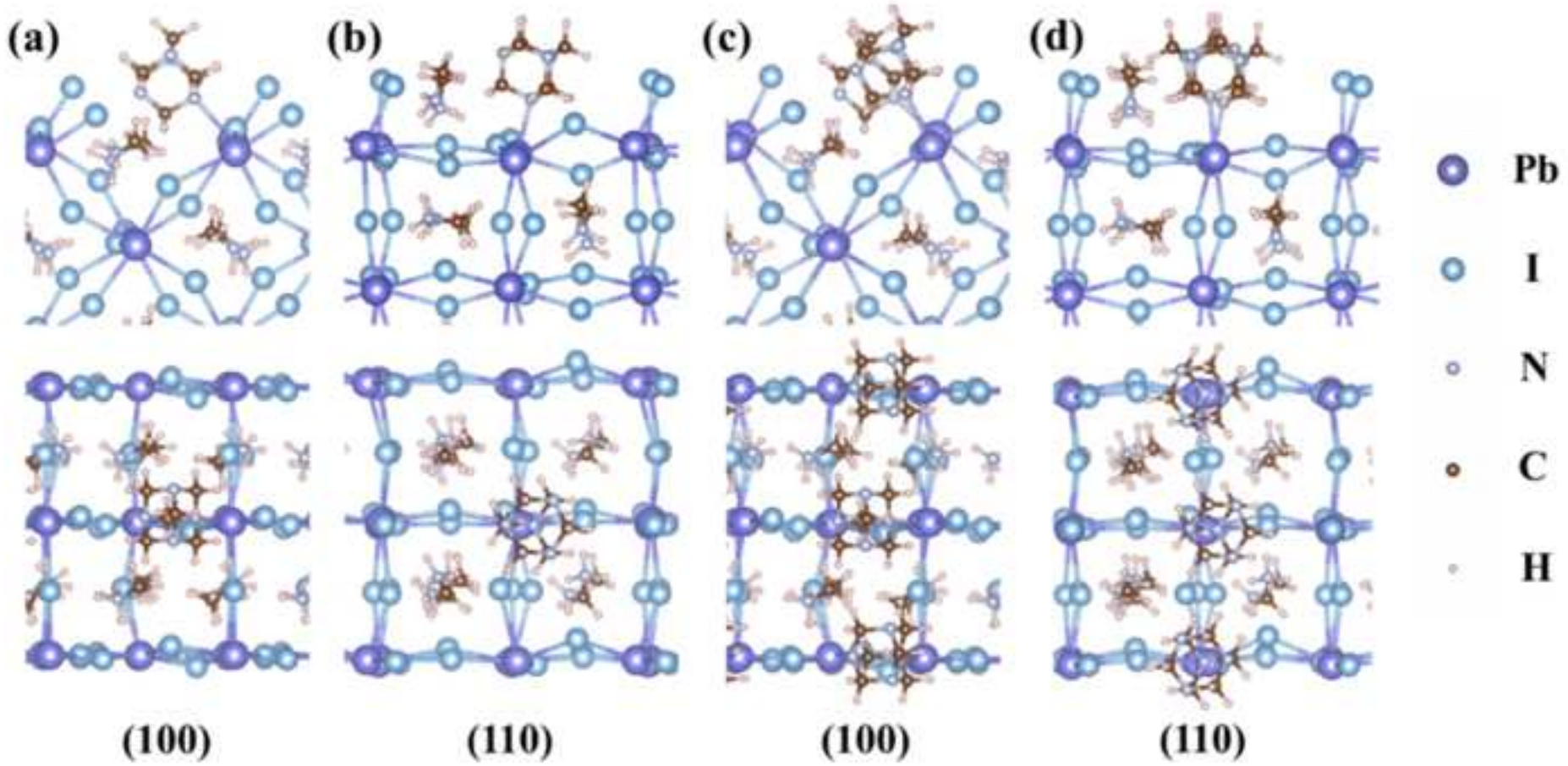

Figure 7

Click here to download high resolution image

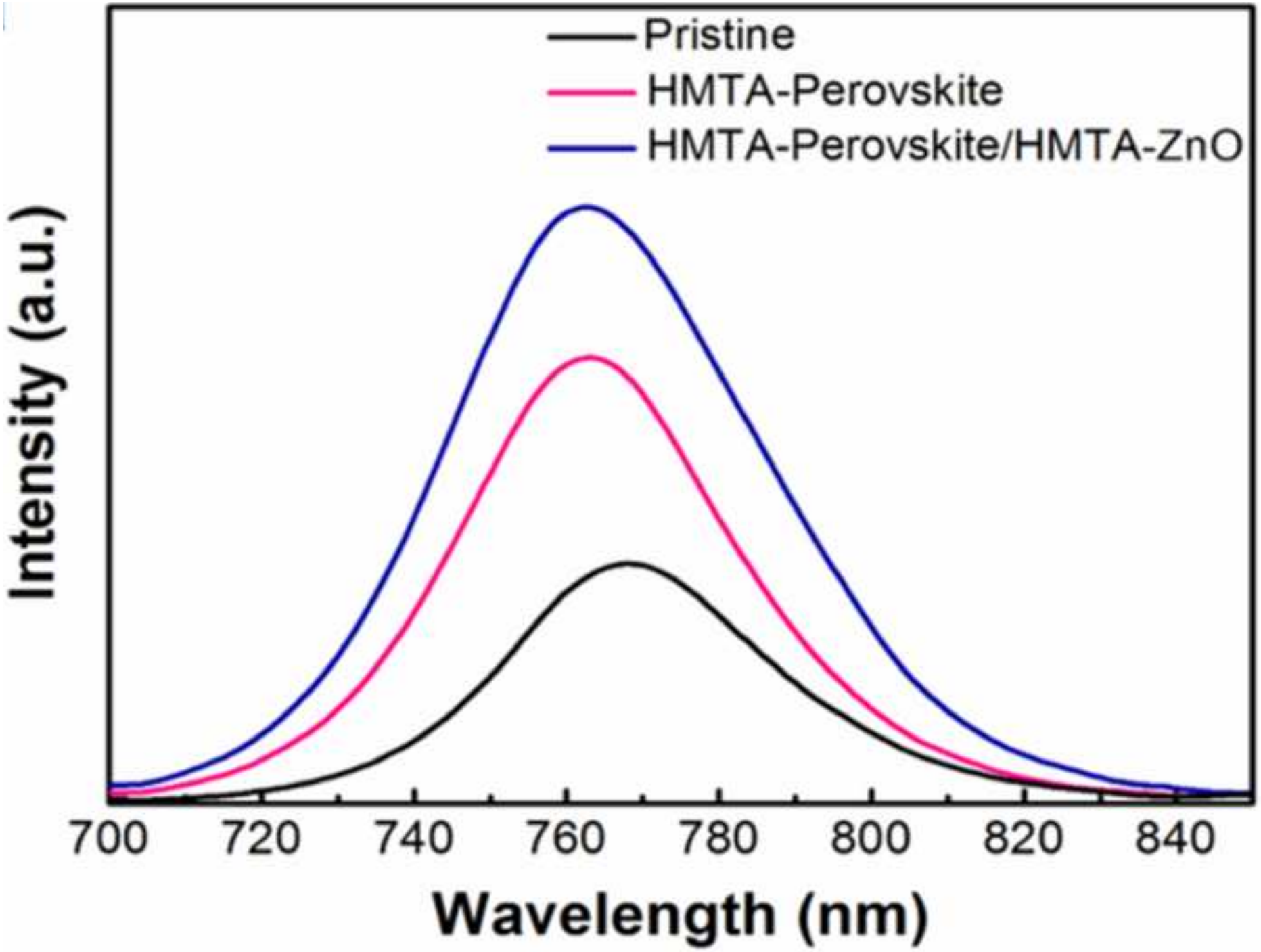

Figure and table captions:

Fig. 1. (a) Schematic illustration of HMTA-assisted grown $CH_3NH_3PbI_3$ neighboring grain structure, in which HMTA coordinates Pb ion on the perovskite surface, as a result leading to orienting of neighboring perovskite grains. (b) Schematic illustration of the planar–structured perovskite solar cell configuration, where a dense and homogeneous perovskite capping layer fully covered onto the HMTA modified ZnO thin electron transport layer.

Fig. 2. XRD patterns of pristine and HMTA-assisted grown $CH_3NH_3PbI_3$ films deposited on ZnO/ITO substrates before and after degradation, which are exposed to ambient air with relative humidity of 55%.

Fig. 3. SEM images of a pristine $CH_3NH_3PbI_3$ (a) and HMTA-assisted grown $CH_3NH_3PbI_3$ (b) films deposited on ZnO/ITO substrates by one-step spin-coating of the corresponding perovskite precursor solutions without or with HMTA additive. (c&d) XPS core level peaks of Pb 4f and N1s of the perovskite and HMTA-perovskite. (e) UPS of bare ZnO and HMTA-ZnO films.

Fig. 4. (a) Cross-sectional SEM image of an optimized device, in which the thickness of HMTA-ZnO, $CH_3NH_3PbI_3$, spiro-MeOTAD, and Ag are 20, 250, 150, and 70 nm, respectively. (b) *J-V* curves measured under AM 1.5 simulated sunlight for the best performing PSCs based on pristine perovskite, HMTA-perovskite, and HMTA-perovskite/HMTA-ZnO films, respectively. (c-f) Histograms of V_{oc}, J_{sc}, *FF*, and *PCE* of 30 cells based on HMTA-perovskite/HMTA-ZnO film, respectively.

Fig. 5. Evolution of normalized device photovoltaic parameters of the unsealed PSCs

based on HMTA- perovskite/HMTA-ZnO films, and pristine perovskite that are stored in ambient air at ~55% humidity in the dark. Error bars represent the standard deviation of the measured PCE for the HMTA- perovskite/HMTA-ZnO (c), and pristine perovskite (d) PSCs (30 devices).

Fig. 6. DFT calculations on the adsorption of the HMTA molecules at two stoichiometric tetragonal $CH_3NH_3PbI_3$ surfaces. Top (upper panel) and side (lower panel) views of the optimized geometries of the tetragonal $CH_3NH_3PbI_3$ surfaces loaded with HMTA. (a& b) One HMTA is adsorbed on the (100) and (110) surfaces, respectively. **(**c&d) Two HMTA molecules adsorbed on the (100) and (110) surfaces, respectively. HMTA is adsorbed on the exposed Pb^{2+} site.

Fig. 7. SS-PL spectra of pristine perovskite, HMTA-perovskite, and HMTA-perovskite/HMTA-ZnO films on ZnO/ITO substrates, respectively.

Table 1 Photovoltaic parameters of PSCs based on pristine perovskite, HMTA-perovskite, and HMTA-perovskite/HMTA-ZnO films under reverse and forward scan directions.

Supplementary Materials

Click here to download Supplementary Materials: Supporting Materials.docx